Glish, S. A. McLuckey, *Anal. Chem.* **62**, 1284 (1990); M. E. Bier, J. C. Schwartz, I. Jardine, G. Stafford, *Proceedings of the Fortieth ASMS Conference on Mass Spectrometry and Allied Topics* (ASMS, Washington, DC, in press).
71. Abbreviations for the amino acid residues are: A, Ala; C, Cys; D, Asp; E, Glu; F, Phe; G, Gly; H, His; I, Ile; K, Lys; L, Leu; M, Met; N, Asn; P, Pro; Q, Gln; R, Arg; S, Ser; T, Thr; V, Val; W, Trp; and Y, Tyr.
72. This article was supported in part by grants from the National Institutes of Health (RR00862 and GM38274) and by funds from the Markey Foundation. We thank R. C. Beavis and R. Wang for their considerable assistance in obtaining experimental results and G. McMilleon for preparing the manuscript.

Detection of Trace Molecular Species Using Degenerate Four-Wave Mixing

Roger L. Farrow and David J. Rakestraw

Spectroscopies that make use of laser light have provided an important tool to modern researchers for the nonintrusive analysis of chemical systems. The strengths and limitations of these spectroscopic techniques often determine the viability of scientific investigations. The unique properties of degenerate four-wave mixing, a nonlinear optical technique, have recently been found to provide powerful capabilities for a wide range of applications.

Optical diagnostic methods provide powerful tools for characterizing the molecular composition and detailed physical properties of chemical systems. The high-intensity, coherent, and spectrally pure radiation provided by lasers, together with recent advances in laser spectroscopy, have revolutionized optical diagnostics. The unique properties of laser techniques allow quantum state–specific measurements to be performed with high temporal and spatial resolution. In addition, laser techniques can be used to provide in situ measurements that can be obtained remotely and nonintrusively. Applications of laser diagnostics are numerous and diverse, ranging from monitoring pollutant formation in combustion processes at high temperatures and pressures, to performing fundamental spectroscopic measurements of isolated molecules in supersonic expansions, to detecting complex macromolecules in biological environments. A variety of spectroscopic techniques are available, each having particular strengths and weaknesses that affect the viability of their application. Important considerations for choosing a technique include sensitivity and dynamic range, applicability to a variety of chemical species, the capability for multidimensional measurements, the capability for quantitative measurements, and the degree of experimental complexity. Among the leading laser diagnostics are spontaneous Raman scattering, laser-induced fluorescence (LIF), ionization spectroscopy, and coherent anti-Stokes Raman scattering (CARS). These techniques have been used extensively and form the cornerstone of much modern scientific research.

During the past several years a relatively mature nonlinear technique, degenerate four-wave mixing (DFWM), has received renewed attention because of its potential role as an optical diagnostic. The wave-mixing process used in DFWM produces a coherent, highly collimated, and spectrally bright signal beam. These properties permit efficient rejection of potential interfering radiation, allow measurements to be obtained remotely, and permit the use of small optical ports for input and output beams. These properties are in contrast to those of linear processes such as spontaneous Raman scattering and LIF, for which the signal radiates nearly isotropically in space, making signal collection and background discrimination more difficult. Although nonlinear processes are generally considered to be weak, DFWM is a completely resonant process and has very high sensitivity for detecting trace molecular species.

Historically, the primary applications of DFWM have been in optical phase conjugation (*1*, *2*) and in the measurement of ultrafast relaxation phenomena in liquids and solids (*3*). The ability to detect trace species with DFWM was first demonstrated for atomic species (*4*), which have strong absorption strengths. The potential for sensitive detection of trace molecular species (which typically have much weaker absorption strengths) was first demonstrated in 1986 by Ewart and O'Leary (*5*), who reported the detection of several OH absorption lines in a methane-air flame at atmospheric pressure. However, several years passed before other research groups began to recognize this potential. During the past 3 years a host of laboratories have begun to investigate the diagnostic capabilities of DFWM; rapid advances both in the fundamental understanding of the technique itself and in new applications that exploit the unique strengths of DFWM have been forthcoming. This article discusses these recent developments and attempts to provide a guide for future users of this promising diagnostic tool. Much of the work discussed will describe applications in combustion environments where the unique properties of DFWM make it particularly valuable. However, the potential applications of DFWM extend far beyond this relatively specific application.

Description of DFWM

Degenerate four-wave mixing involves the interaction of three input beams of identical frequency ω with a nonlinear medium to produce a fourth coherent signal beam of the same frequency ω. A schematic diagram of a commonly used laser beam geometry is shown in Fig. 1A. In this geometry, two pump beams with electric field vectors $\mathbf{E}_f$ (forward) and $\mathbf{E}_b$ (backward) are coaxial and counterpropagating, and they cross a third beam, $\mathbf{E}_p$ (probe), at an angle θ. The nonlinear polarization of the medium couples these three beams through the third-order susceptibility tensor $\chi^{(3)}$ to generate a fourth beam $\mathbf{E}_s$ that counterpropagates collinear with $\mathbf{E}_p$. This geometry meets the phase-matching requirements for all angles θ and has the unique property that $\mathbf{E}_s$ is proportional to the complex conjugate of $\mathbf{E}_p$.

A qualitative physical description of the four-wave mixing interaction is helpful in understanding the generation of $\mathbf{E}_s$. An interference of $\mathbf{E}_p$ with $\mathbf{E}_f$ and $\mathbf{E}_b$ gives rise to an optical fringe pattern in the sample such that the intensity of the light varies sinusoidally in the beam overlap region. The fringe spacing Λ is given by

$$\Lambda = \lambda_p/2\sin(\theta/2) \qquad (1)$$

where λ_p is the wavelength of the interfering radiation. In an absorbing medium, this spatial oscillation in intensity results in a corresponding variation in the concentration of excited and ground states. These alternating regions are characterized by a varying index of refraction and a varying absorption coefficient and therefore form a Bragg grating. This volume diffraction grating produced by the interference of $\mathbf{E}_p$ with $\mathbf{E}_f$ and $\mathbf{E}_p$ with $\mathbf{E}_b$ then results in the scattering of $\mathbf{E}_b$ and $\mathbf{E}_f$, respectively, producing the signal wave $\mathbf{E}_s$. The interference

---

The authors are at the Combustion Research Facility, Sandia National Laboratories, Livermore, CA 94551.

of $\mathbf{E}_p$ with $\mathbf{E}_f$ is shown schematically in Fig. 1B. Because all four beams are of the same frequency, a strong resonant enhancement of the DFWM signal occurs whenever ω matches an allowed molecular transition. Therefore, examination of $\mathbf{E}_s$ as a function of input laser frequency will result in the sensitive mapping of the atomic and molecular species by absorption in the interaction region.

A typical experimental configuration for conducting DFWM experiments is shown in Fig. 2. In this example, a tunable source of visible radiation is provided by a dye laser that is pumped by an injection-seeded, frequency-doubled Nd:YAG (neodymium:yttrium-aluminum-garnet) laser having a pulse duration of 10 to 15 ns. The output of the visible dye laser can then be used to generate ultraviolet or infrared radiation by frequency doubling or mixing. The desired output is spatially filtered to improve the laser beam profile. The output is passed through a photo-elastic modulator crystal and polarizer to allow active control of the transmitted intensity with a computer. At this point a beam splitter is used to produce the probe and forward pump beams, which are crossed at a small angle (typically 1° to 4°) and intersect in the medium to be studied. A second beam splitter placed in the probe beam path is used to extract the phase conjugate signal. The signal beam is directed to a convenient detection location often several meters away (to improve rejection of stray light not generated by the wave-mixing process). Before detection the signal beam is passed through a spatial filter consisting of a lens and a pinhole ~100 μm in diameter before being directed to the appropriate photodetector.

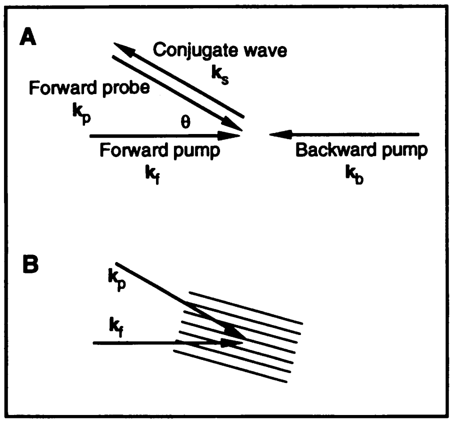

Fig. 1. (**A**) Schematic diagram of the phase-conjugate DFWM beam geometry. The wave vectors, $\mathbf{k}_i$, correspond to the electric field vectors, $\mathbf{E}_i$. (**B**) Schematic drawing of the large-spacing grating (Δk) formed from the interference of the forward pump and the probe laser beams. The small-spacing grating ($2k$) formed between the forward probe and the backward pump laser beams is not shown.

Detection of Molecular Species

A DFWM spectrum is illustrated in Fig. 3. This DFWM spectrum shows a section of the NO A $^2\Sigma^+ \leftarrow$ X $^2\Pi$ band system near 226 nm. The NO was thermally generated in an H_2-O_2-N_2 diffusion flame operating at atmospheric pressure. We were able to obtain spectra in this flame with signal-to-noise ratios greater than 2000:1 where the NO concentrations were estimated to be ~400 ppm (*6*). The pump and probe laser beams were unfocused but collimated, with beam diameters of ~1 mm and relatively modest pulse energies of ~20 μJ (0.2 MW/cm^2). Also shown in Fig. 3 is a simulated spectrum based on the model of Abrams *et al.* (*7*). DFWM measurements of other important combustion species, including OH (*5, 8, 11*), NH (*9, 12*), NO_2 (*13*), and CH (*14*), have been reported. Our early experiments involving OH demonstrated that the signal intensity could be described under conditions of saturation by the simple relation

$$I_{DFWM} \propto (\Delta N^2 \mu_{12}^4) \qquad (2)$$

where ΔN is the population difference be-

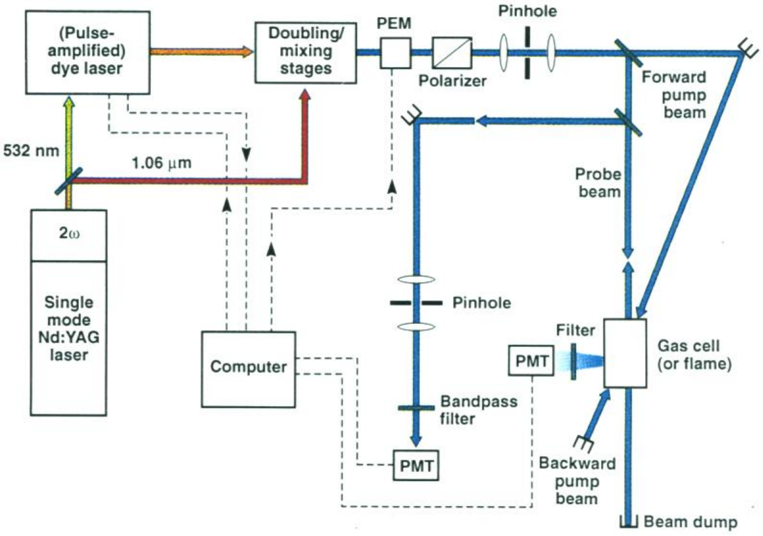

Fig. 2. Schematic diagram of a typical experimental configuration used for performing the DFWM measurements. The specific optics and detectors vary depending on the frequency of the radiation used. PEM, photoelastic modulator; PMT, photomultiplier tube.

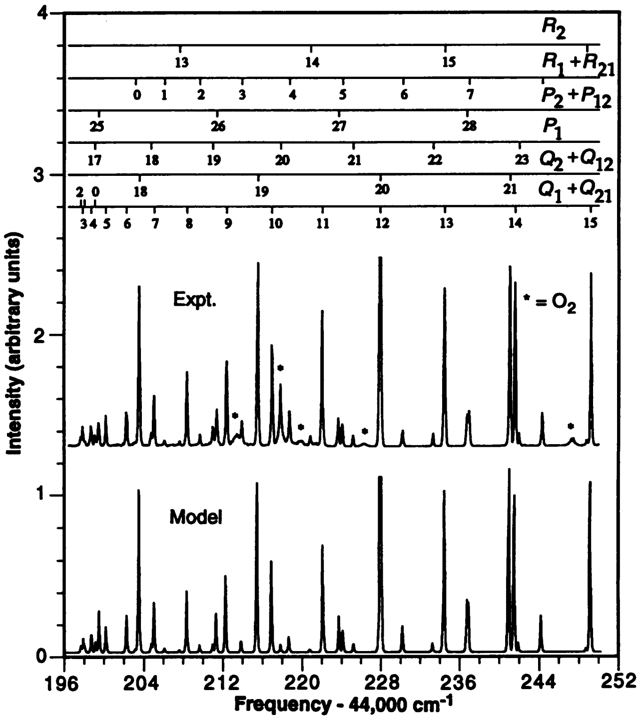

Fig. 3. Experimental (upper curve) and simulated spectra (lower curve) of the A $^2\Sigma^+ \leftarrow$ X $^2\Pi$ band of NO near the bandhead region of the Q_1 + Q_2 branches at 226 nm. The spectrum was obtained in an H_2-O_2-N_2 diffusion flame. The branches of the A-X transition are indicated at the top of the figure. The experimental spectrum is offset for clarity. The peak near 44,228 cm^{-1} has been plotted offscale to enhance the display of weaker lines; its intensity relative to that of the $Q_2(18)$ + $Q_{12}(18)$ is 3.1 and 3.7 for experiment and theory, respectively. Asterisks mark several O_2 transitions observed experimentally that were not included in the simulation. A detailed description of the simulated spectra can be found in (*6*).

tween the probed levels and μ_{12} is the transition dipole moment (*8*). This relation has been confirmed by other laboratories for OH (*10, 11*) and also has been shown to be valid for NH (9), CH (*14*), and NO (*15*). By the use of this relation local temperatures have been determined from the relative population of rotational levels in a variety of combustion environments and laboratory vessels. These experiments have collectively shown the ease with which DFWM can be applied to detect trace species (that is, concentrations of 10^{10} to 10^{12} molecules per cubic centimeter).

The detection of several stable species at slightly higher concentrations has been examined by Meijer and Chandler (*16*), using weak electronic absorptions in the ultraviolet spectral region for resonance enhancement of the DFWM process. These experiments made use of overlaps of a tunable excimer laser with molecular transitions near 193 and 248 nm: H_2 and H_2O were detected by means of two-photon transitions, and CO and O_2 were detected by means of weak one-photon transitions. In order to compensate for the weaker absorption strengths, Meijer and Chandler used higher laser intensities obtained by focusing the laser beams. They utilized a four-wave mixing geometry in which all three input beams propagated in the same direction, and the beams were conveniently generated by the placement of a mask in front of the output of the excimer laser.

The applications discussed to this point have involved the use of electronic transitions for resonance enhancement. However, the DFWM interaction depends on absorption rather than emission, thereby allowing the efficient detection of molecular transitions that have long fluorescence lifetimes or low fluorescence quantum yields (which are not easily detected with emission techniques). We have exploited this property to detect molecules by infrared absorptions in the ground electronic state (*17*). Initial measurements involving the HF(1-0) and HCl(1-0) transition have demonstrated relatively high sensitivities of 10^{10} molecules/cm^3. Experiments are currently under way in which infrared DFWM is being used to detect polyatomic molecules with absorptions in the 2- to 4-μm range. The ability to use purely rovibrational transitions to detect molecular species marks a significant advance because it extends the use of DFWM to a large class of molecules that are difficult or impossible to probe by electronic transitions.

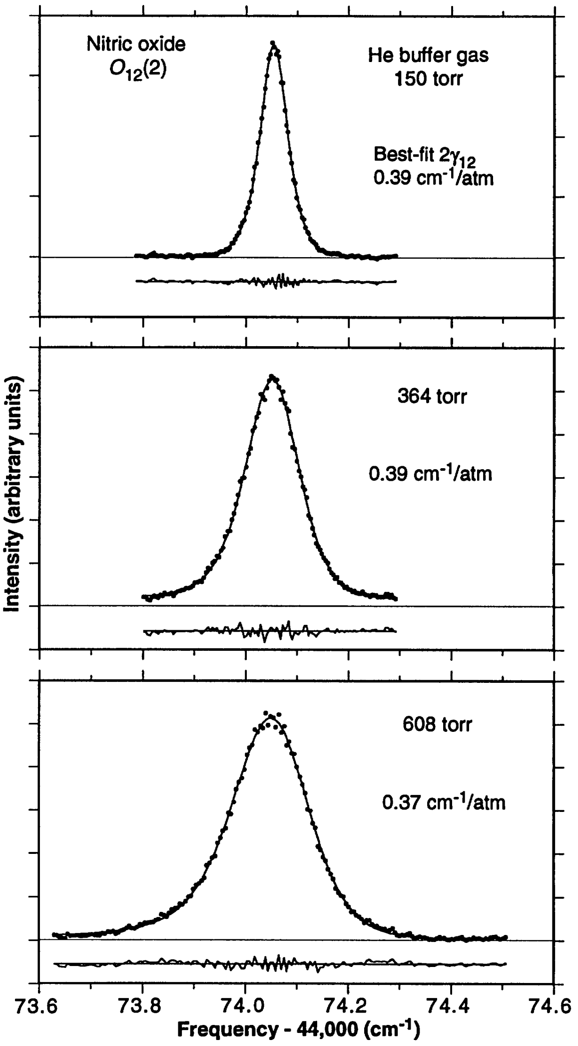

Fig. 4. A comparison of experimental (symbols) and theoretical (curves beneath symbols) DFWM line shapes for the $O_{12}(2)$ transition of NO in various pressures of He at 295 K. The NO partial pressure was <70 mtorr to ensure that the peak absorption was below 3%. The theoretical curves are based on a moving-absorber model in which the collisional broadening parameter γ_{12} was varied for best fit, yielding the indicated values. These are in excellent agreement with the value for $2\gamma_{12}$ determined from LIF data, which was 0.38 ± 0.015 cm^{-1}/atm. [The Doppler width of $O_{12}(2)$ is 0.099 cm^{-1} at room temperature.]

Although DFWM has not been shown to match the highest sensitivities achievable with LIF or ionization techniques, the coherent nature of the DFWM signal and its ability to detect many molecules by infrared transitions provide special capabilities that will make DFWM the preferred technique in many applications. This potential has provided the motivation for further investigation of other applications and of the fundamental properties of DFWM in more detail.

Interpretation of Spectral Intensities

Spectral intensities obtained with DFWM are proportional to the squared modulus of the complex third-order susceptibility tensor $|\chi^{(3)}|^2$. As the input laser frequency is tuned through absorption lines in the medium, perturbations in the index of refraction and absorption coefficient are produced that correspond to resonances in $\chi^{(3)}$. Thus, the DFWM spectrum often resembles the square of the absorption spectrum of the medium. The relation between DFWM and absorption spectra is analogous to that between CARS and spontaneous Raman spectra. Moreover, in both nonlinear techniques, additional spectral complexity arises from the dependence on the squared modulus of $\chi^{(3)}$, which implies a coherent addition of transition amplitudes. This property leads to constructive (or destructive) interferences in the intensities of overlapping lines and can result in asymmetric line shapes. An example of the first effect is seen in Fig. 3, where a chance overlap between transitions at 44,228.0 cm^{-1} produces an anomalously intense line (plotted off scale).

The spectral profile of an isolated line observed with DFWM is also somewhat more complicated than the simple square of the absorption line shape. The fact that DFWM signals are generated from the resonant interaction of three laser fields results in a line shape proportional to the cube of the absorption profile (that is, a Lorentzian profile raised to the third power) for slowly moving absorber molecules at low laser intensities (*7*):

$$I_{\mathrm{DFWM}} \approx \alpha_0^2 \frac{1}{1+\delta^2} L^2 \frac{4I_p(I/I_{\mathrm{sat}})^2}{[1+(4I/I_{\mathrm{sat}})]^3} \quad (3)$$

Here the frequency-dependent saturation intensity is given by $I_{\mathrm{sat}} = I^0_{\mathrm{sat}}(1 + \delta^2)$, where I^0_{sat} is the line-center value, L is the interaction length, α_0 is the line-center

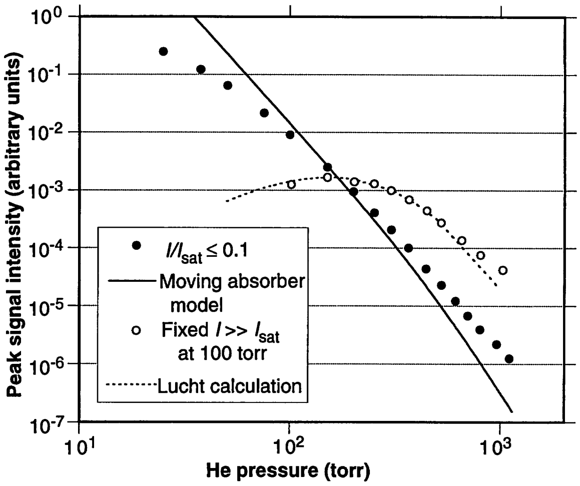

Fig. 5. A comparison of the variation with foreign-gas pressure of experimental (symbols) and theoretical (solid line) DFWM peak intensities for the $O_{12}(2)$ transition of NO. The filled symbols indicate measurements made with low laser intensities; the open symbols were obtained with a fixed, high laser intensity. Scaling factors have been applied to the plots for comparison purposes.

field absorption coefficient, I and I_p are the respective pump and probe intensities, and δ is the frequency detuning from resonance divided by the coherence dephasing width γ_{12}. The Lorentz-cubed line shape occurs for $I << I_{sat}$, where the second denominator is approximately 1. In this case the DFWM profile is narrower than the absorption line by roughly a factor of 2.

Absorber motion cannot be neglected when the attendant Doppler shifts are significant compared to the homogeneous linewidth. Selection of particular groups of molecules according to velocity can occur if the input beams are propagating in different directions, because only the groups that are (most nearly) resonant with all three beams contribute effectively to the signal. In the phase-conjugate geometry, only molecules with near-zero velocity along the beam propagation direction simultaneously interact with the counterpropagating pump beams and the probe beam for small angles of θ, giving rise to a sub-Doppler linewidth. Analytic expressions for the phase-conjugate line shape have been derived in the limit of low laser intensity (*7*). We have tested these expressions for NO as a function of the ratio between the collision linewidth γ_{12} and ku_0, the Doppler shift for the most probable molecular speed u_0. We measured spectra of NO in various pressures of He buffer gas, using a high-resolution (~0.004 cm^{-1} full-width) laser tuned near 226 nm; examples are compared to the moving-absorber theory in Fig. 4. The comparisons demonstrate quantitative agreement between theory and experiment for γ_{12}/ku_0 ranging from 0.64 to 2.6. In addition, Brown *et al.* (*18*) found that the theory successfully described DFWM line shapes of OH measured in a flame, where γ_{12}/ku_0 was ≈ 0.5.

Although collisional broadening plays an important role in determining the line shape, it can also have a dramatic effect on DFWM line intensities. The extent of the effect depends sensitively on the degree of saturation induced by the measurement process. (Saturation is a reduction of the difference in population between upper and lower states due to laser excitation; full saturation corresponds to an induced population difference of zero and results in loss of signal.) In the absence of saturation, line intensities are expected to vary as γ_{12}^{-x}, where x ranges from 4 to 6 (depending on γ_{12}/ku_0). However, in the limit of full saturation, intensities should be independent of γ_{12} (*7, 19*). Fortunately, the strong dependence in the absence of saturation is rarely observed in practice, because of the difficulty of completely eliminating saturation. As indicated by the filled symbols in Fig. 5, we observe an intensity dependence ranging from γ_{12}^{-2} to γ_{12}^{-4}, measured by varying the pressure p of the He buffer gas ($\gamma_{12} \propto p$). As expected, this dependence is less strong than predicted by the moving-absorber theory (*7*) (solid curve in Fig. 5), which ignores saturation. To examine the importance of saturation, we repeated the measurements using a much higher laser intensity. In this case, saturation was significant for the lower pressures, and the corresponding intensities were nearly independent of p (open symbols rescaled to compare with the unsaturated case). Although an analytic theory does not exist for the case of strong saturation and nonzero γ_{12}/ku_0, a calculation (broken curve) performed by numerically solving (*20*) the density matrix equations describing DFWM agrees remarkably well with the experimental result.

Imaging of Species Distributions

The potential use of DFWM to do real-time processing of electromagnetic fields in two dimensions has long been recognized and has generated tremendous interest in areas such as information processing and photolithography (*1*). Most of these applications have involved the external modulation of the radiation, which is then directed into a uniform nonlinear medium used for optical phase conjugation. It was recently demonstrated by Ewart and co-workers (*21*) that, by using uniform laser beams, DFWM could also be used to measure the spatial inhomogeneities in a medium. They successfully measured two-dimensional distributions of atomic sodium in a flame (*21*). We have performed similar measurements for the molecular species OH (*22*). The high sensitivity combined with the low laser intensity requirements of DFWM make it ideally suited for two-dimensional measurements with single laser shots of ~10-ns duration.

The geometry used for these experiments is shown in Fig. 6 (several changes have been made to the configuration shown in Fig. 2). A cylindrical telescope is used to form the pump beams into a laser sheet. The forward and backward pump beams define a plane in the sample which is then intersected by a circular probe beam at an angle of 10° to 45°, creating an elliptical intersection. In an effort to maximize the signal to background ratio, we also modified the configuration of the beam polarizations. The backward pump beam is oriented at 90° with respect to the forward pump beam and the probe beam. The generated signal beam will therefore be polarized parallel to the backward pump, allowing efficient discrimination against the scatter of the forward pump beam and probe beam with a polarizer.

An example of a single-shot image generated by OH molecules in an axisymmetric methane-air diffusion flame is shown in Fig. 7. The observed OH distribution reflects the shape of the fuel-air reaction zone and the effects of diffusion of the OH toward the air side. To measure quantitatively the OH number density from this image, temperature information would be necessary. However, changes in the population of the level probed by the $P_2(8)$ transition used in the experiment are small (<12%) for temperatures of 1200 to 2400 K. By comparing signal intensities of images produced using transitions from different rotational levels, one can derive a two-dimensional temperature map of the probed region. Ewart and Kaczmarek have recently reported the two-dimensional mapping of temperature in a flame by recording images from three different rotational transitions of OH (*23*). These workers took advantage of the stable flame used in their experiment by recording pulse-averaged images for each rotational transition sequentially in time. Creating a two-dimensional temperature map of a dynamic system would require the simultaneous use of two laser frequencies and two imaging cameras.

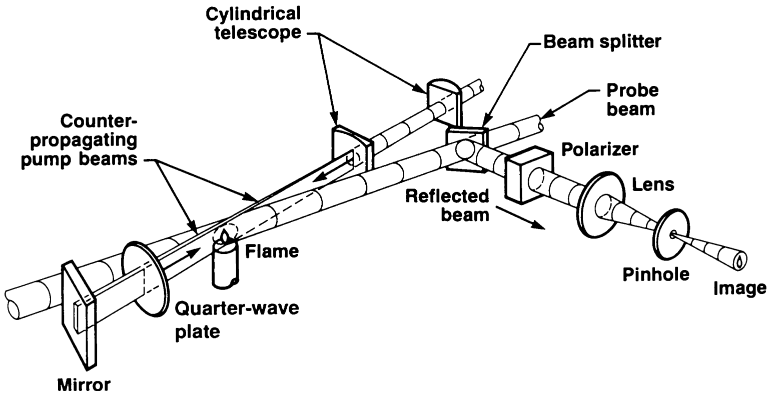

Fig. 6. Schematic diagram of a beam and detection geometry used in the DFWM imaging experiments. After propagating through the pinhole, the signal image is directed to an unintensified charge-coupled device camera. This geometry enables very efficient discrimination against highly luminous backgrounds such as a highly sooting diffusion flame.

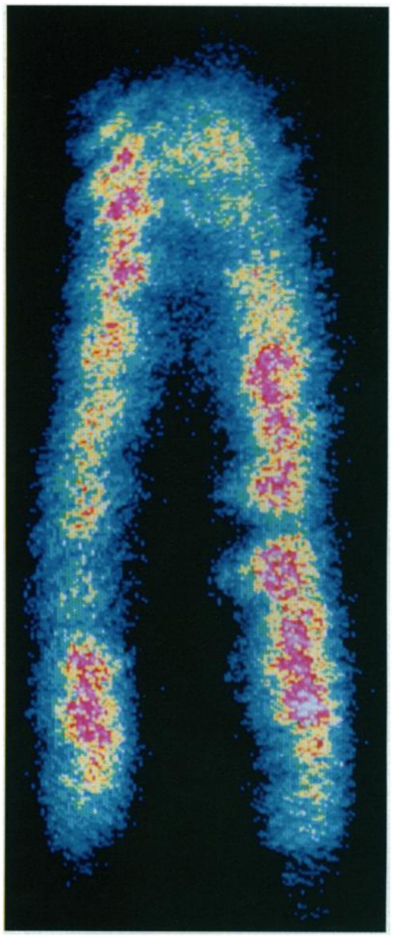

Fig. 7. Image of the OH intensities produced by DFWM in an axisymmetric methane-air diffusion flame. The image results from the intersection of a flat laser sheet 300 μm thick and the OH distribution in the flame. The OH distribution is a maximum in the flame front and can be seen to surround the central methane stream propagating from the bottom of the figure. The concentration of OH is color-coded with white and black representing the highest and lowest concentrations, respectively.

Multiplexed Detection

The DFWM spectrum shown in Fig. 3 was generated by scanning the frequency of a narrow band laser across a portion of the A $^2\Sigma^+ \leftarrow X\ ^2\Pi$ band system of NO. By making use of the steady-state nature of the system under investigation, the DFWM signals resulting from multiple laser pulses were averaged for each small frequency interval. The final spectrum can therefore take many minutes to a fraction of an hour to obtain. However, many spectroscopic applications involve probing fluctuating systems for which time-averaged measurements are not acceptable. Therefore, it is important to be able to make "instantaneous" measurements of physical and chemical parameters. Broadband CARS is an excellent example of a multiplexed technique (*24*) that can be used in the accurate determination of temperature and in some cases in the measurement of concentrations of major species with single laser pulses ($<$10 ns).

Perfecting the ability to obtain high-quality DFWM spectra with a single laser pulse will be an extremely important advance. Ewart and co-workers have made significant progress in this area both theoretically (*25, 26*) and experimentally (*27*). Initial experiments involved measurements of the sodium D lines near 590 nm. Broadband visible light was produced with a "modeless" laser (*28*) with a full width at half maximum covering approximately 2 nm. The experimental arrangement was very similar to that shown in Fig. 2 except that in this case the DFWM signal beam was dispersed through a spectrograph and detected with a two-dimensional diode array. Ewart's group is currently extending the measurements to examine the OH radical in the ultraviolet (*29*). To date these experiments have proven to be challenging because of the difficulty in producing broadband radiation that has sufficient spectral brightness to drive the nonlinear process. To address this problem, Yip, Danehy, and Hanson (*30*) have conducted similar experiments on OH in which the spectrograph has been replaced with an etalon. The etalon provides high spectral dispersion, permitting the use of a laser with smaller spectral bandwidth. These researchers recently reported temperature measurements in flames based on the use of this method (*30*).

Although initial multiplexed DFWM measurements have proven somewhat difficult, the utility of this method is very high. The ability to make instantaneous measurements of concentration and temperature of multiple trace molecular species provides a long-awaited tool facilitating the study of turbulent chemical systems.

Applications to Molecular Spectroscopy

In addition to the many analytical applications of DFWM, several recent experiments have shown that four-wave mixing techniques can also be an extremely powerful tool for pure molecular spectroscopy. One long-recognized property of DFWM, the sub-Doppler nature of the line shapes when the phase-conjugate geometry is used, can be used to significantly improve spectral resolution and therefore assist in understanding complex spectra consisting of closely spaced transitions. A comparison of the sub-Doppler DFWM and the inhomogeneous broadened LIF line shapes is given in Fig. 8. This increase in resolution afforded by DFWM is accompanied by a decrease in sensitivity because only a small subset of molecules can participate in the nonlinear process (which furthermore has a quadratic dependence on number density). Under the experimental conditions used for Fig. 8, only ~3% of the room-temperature NO molecules significantly contributed in the DFWM signal generation. If no benefit is gained from this increased resolution, higher sensitivity can be gained through the use of a laser bandwidth comparable to the Doppler width or through the use of a forward beam geometry.

Another important spectroscopic application is the use of four-wave mixing techniques for performing excited-state spectroscopy. The detection scheme used by Vacarro and co-workers (*31*) is illustrated in Fig. 9. A pump laser generates an excited-state population that is then probed by means of a downward transition to a highly excited vibrational level of the ground state by DFWM. This detection scheme is a modification of stimulated emission pumping (SEP), first demonstrated by Field and

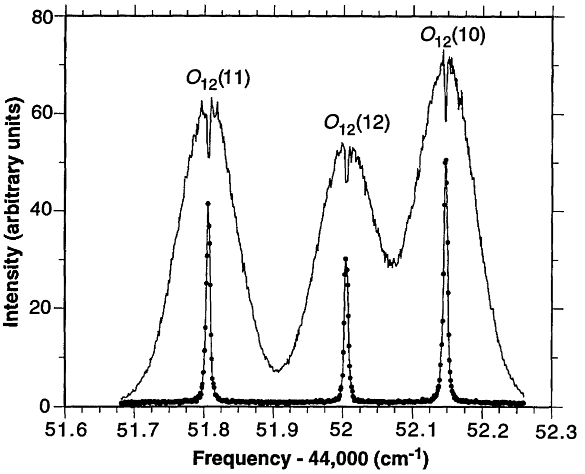

Fig. 8. Comparison between experimental DFWM spectral peaks (connected symbols) and the simultaneously measured fluorescence excitation spectra (solid curve) forming the O_{12} bandhead of the NO A-X transition. The sub-Doppler nature of the DFWM line shapes measured in the phase-conjugate geometry is clearly evident.

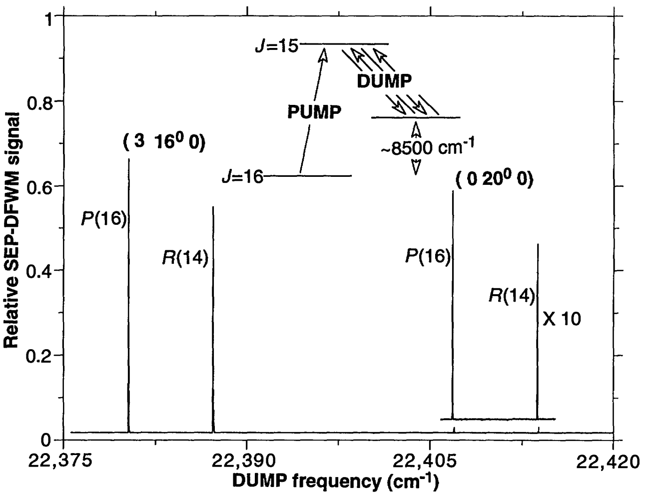

Fig. 9. SEP-DFWM spectrum recorded for gaseous CS_2 at a total sample pressure of ~0.030 torr. DUMP, beam dump; PUMP, pump beam. The pump laser frequency was tuned to coincide with a single rovibronic transition of CS_2 10V band [*P*(16) at 30893.53 cm^{-1}], thereby producing a state-selected ensemble of electronically excited molecules. As the wavelength of the DFWM probe laser is scanned in the vicinity of 24,400 cm^{-1} two pairs of resonances are observed. These features can be attributed to the *R*(14) and *P*(16) rotational lines for vibronic transitions originating from the single rotational-vibrational level prepared in the excited electronic state and terminating on two highly excited vibrational states of the ground state. The notation (v_1, $v_2^{\ell 2}$, v_3) [that is, (3 16° 0) and (0 20° 0)] indicates the nominal assignment for each of these vibrational states in terms of normal modes (v_1 = symmetric stretch, v_2 = doubly degenerate bend, and v_3 = antisymmetric stretch. [Courtesy of P. H. Vacarro]

co-workers (*32*), which relied on the observation of fluorescence depletion to detect the downward transitions. The SEP-DFWM approach has the distinct advantage that it is a null-background technique and is therefore a very sensitive spectroscopic method, as illustrated in Fig. 9 for CS_2.

A variation of the SEP-DFWM method for performing excited-state spectroscopy has been demonstrated by Buntine, Chandler, and Hayden (*33*) for the (B $^3\Pi^+_{0u}$ ← X $^1\Sigma^+_g$) transition in I_2. This approach incorporates one laser frequency to form an excited-state grating, and a second frequency is used to probe the grating. This technique has appropriately been designated two-color, laser-induced grating spectroscopy (TC-LIGS). The double resonance selectivity afforded by the TC-LIGS scheme eliminates potential complications of SEP-DFWM where the DFWM probing could detect ground-state transitions. This selectivity, however, comes at the expense of reducing the phase matching simplicity of the degenerate wavelength experiments. Recent experiments of Butenhoff and Rohlfing (*34*) have demonstrated that the sensitivity of TC-LIGS is such that this technique can be successfully applied to transient species in molecular beams. Butenhoff and Rohlfing have investigated the application of TC-LIGS to C_3 and SiC_2 after laser vaporization of graphite or silicon carbide into supersonic expansions.

The uses of four-wave mixing techniques in molecular spectroscopy are just beginning to emerge. It seems clear, however, that the ability to conduct sensitive, high-resolution spectroscopy on molecular transitions that are not easily probed with the use of fluorescence or ionization techniques can fill an important void in this field.

Conclusions

The use of DFWM as a diagnostic technique is in the early stages of development. However, its unique features, which include high spatial and temporal resolution, sensitive detection of trace species by means of electronic and vibrational transitions, and a coherent signal beam, are generating widespread interest. We have described some applications in combustion diagnostics as well as chemical physics, but the potential applications have just begun to be addressed. As the capabilities and limitations of DFWM are better understood, scientists and engineers in diverse disciplines are likely to make increasing use of this potentially powerful tool for probing chemical systems.

REFERENCES AND NOTES

1. R. A. Fisher, Ed., *Optical Phase Conjugation* (Academic Press, New York, 1983).
2. J. F. Reintjes, *Nonlinear Optical Parametric Processes in Liquids and Gases* (Academic Press, Orlando, FL, 1984).
3. H. J. Eichler, D. Pohl, P. Gunter, *Laser-Induced Dynamic Gratings* (Springer Series in Optical Sciences vol. 50, Springer, New York, 1986).
4. P. Ewart and S. V. O'Leary, *J. Phys. B* **15**, 3669 (1982); *ibid.* **17**, 4609 (1984).
5. ______, *Opt. Lett.* **11**, 279 (1986).
6. R. L. Vander Wal, R. L. Farrow, D. J. Rakestraw, in *Proceedings of the Twenty-Fourth International Symposium on Combustion* (Combustion Institute, Pittsburgh, in press).
7. R. L. Abrams, J. F. Lam, R. C. Lind, D. G. Steel, P. F. Liao, in (*1*), p. 211.
8. T. Dreier and D. J. Rakestraw, *Opt. Lett.* **15**, 72 (1990).
9. ______, *Appl. Phys. B* **50**, 479 (1990).
10. M. Winter and P. P. Radi, *Opt. Lett.* **17**, 320 (1992).
11. ______, A. Stampanoni, in *Proceedings of the Twenty-Fourth International Symposium on Combustion* (Combustion Institute, Pittsburgh, in press).
12. D. J. Rakestraw, T. Dreier, L. R. Thorne, in *Proceedings of the Twenty-Third International Symposium on Combustion* (Combustion Institute, Pittsburgh, 1991), p. 1901.
13. B. A. Mann, S. V. O'Leary, A. G. Astill, D. A. Greenhalgh, *Appl. Phys. B* **54**, 271 (1992).
14. D. S. Green, S. Williams, R. N. Zare, *J. Am. Chem. Soc.*, in press.
15. R. L. Farrow, D. J. Rakestraw, T. Dreier, *J. Opt. Soc. Am. B*, in press.
16. G. Meijer and D. W. Chandler, *Chem. Phys. Lett.* **192**, 1 (1992).
17. R. L. Vander Wal *et al.*, *ibid.* **191**, 251 (1992).
18. M. S. Brown, L. A. Rahn, T. Dreier, *Opt. Lett.* **17**, 76 (1992).
19. For this discussion we have assumed that $\gamma_1 \propto \gamma_{12}$, where $\gamma_1 = 1/T_1$ is the linewidth contribution from the coherence lifetime T_1.
20. R. P. Lucht, R. L. Farrow, D. J. Rakestraw, in preparation.
21. P. Ewart, P. Snowdon, I. Magnusson, *Opt. Lett.* **14**, 563 (1989).
22. D. J. Rakestraw, R. L. Farrow, T. Dreier, *ibid.* **15**, 709 (1990).
23. P. Ewart and M. Kaczmarek, *Appl. Opt.* **30**, 3996 (1991).
24. A. C. Eckbreth, *Laser Diagnostics for Combustion Temperature and Species* (Abacus, Cambridge, MA, 1988).
25. J. Cooper, A. Charlton, D. R. Meacher, P. Ewart, G. Alber, *Phys. Rev. A* **40**, 5705 (1989).
26. D. R. Meacher, A. Charlton, P. Ewart, J. Cooper,

G. Alber, *ibid.* **42**, 3018 (1990).
27. P. Ewart and P. Snowdon, *Opt. Lett.* **15**, 1403 (1990).
28. P. Ewart, *Opt. Commun.* **55**, 124 (1985).
29. I. P. Jefferies, A. J. Yates, P. Ewart, in *Coherent Raman Spectroscopy: Applications and New Developments*, E. Castellucci, Ed. (World Scientific, Singapore, in press).
30. B. Yip, P. M. Danehy, R. K. Hanson, *Opt. Lett.* **17**, 751 (1992).
31. Q. Zhang, S. A. Kandel, T. A. W. Wasserman, P. H. Vacarro, *J. Chem. Phys.* **96**, 1640 (1992).
32. C. E. Hamilton, J. L. Kinsey, R. W. Field, *Annu. Rev. Phys. Chem.* **37**, 493 (1986).
33. M. A. Buntine, D. W. Chandler, C. C. Hayden, *J. Chem. Phys.* **97**, 707 (1992).
34. T. J. Butenhoff and E. A. Rohlfing, *ibid.*, p. 1595.
35. We thank the many researchers cited in this article for making their work available to us at early stages. We especially thank P. H. Vacarro for providing us with Fig. 9. This work was supported by the U.S. Department of Energy, Office of Basic Energy Sciences, Division of Chemical Sciences and Office of Industrial Technologies, Division of Advanced Industrial Concepts, and the Gas Research Institute.

From Molecules to Cells: Imaging Soft Samples with the Atomic Force Microscope

M. Radmacher, R. W. Tillmann, M. Fritz, H. E. Gaub*

Since its invention a few years ago, the atomic force microscope has become one of the most widely used near-field microscopes. Surfaces of hard samples are imaged routinely with atomic resolution. Soft samples, however, remain challenging. An overview is presented on the application of atomic force microscopy to organic samples ranging from thin ordered films at molecular resolution to living cells. Fundamental mechanisms of the image formation are discussed, and novel imaging modes are introduced that exploit different aspects of the tip-sample interaction for local measurements of the micromechanical properties of the sample. As examples, images of Langmuir-Blodgett films, which map the local viscoelasticity as well as the friction coefficient, are presented.

Traditional microscopes use waves, such as light or electrons, and suitable imaging optics to create a two-dimensional projection of certain properties (such as the local absorbency) of the object. In near-field microscopes (*1*), a small probe is brought into close proximity to the object and, by guiding the probe over the surface, a three-dimensional relief of the object is obtained that reflects the nature of the local interaction between the probe and the sample. In the most prominent example of such microscopes, the scanning tunneling microscope (STM) (*2*), the probe is guided such that a given tunneling current between probe and the sample remains constant. In the atomic force microscope (AFM) (*3*) (Fig. 1), force fields between the probe and the sample are used to guide the probe over the surface (*4*). The use of forces has proved to be a general approach and has made the scanning probe techniques relevant to a wide range of applications (*5–14*). It also allows imaging of nonconducting materials under various ambient conditions such as physiological buffer solutions, making it a very promising tool for life sciences (*1, 15–22*). The AFM images reflect, in the widest sense, the local mechanical properties of the sample (*14*). In the case of hard samples, the image is dominated by the surface topology and the tip geometry, whereas for soft samples the viscoelastic properties of the sample contribute significantly to the image formation (*23*). As such, the AFM may be most easily described as the instrumental evolution of the tactile sense toward the delicacy and dimensions of individual molecules.

Imaging with the AFM

Although the AFM shares essential features with the profilometer (*24*), an established instrument which measures the surface topology of hard surfaces by scratching it with a stylus, the AFM has, like all near-field microscopes, historically evolved from the STM (*2*). Like the STM, the AFM uses piezo ceramics to position the probe or sample to an accuracy of fractions of atomic diameters (*25*). In the AFM, the probing tip is mounted at the end of a soft cantilever spring, which is normally made by silicon micromanufacturing (*26*). During imaging, suitable electronics are used to guide the tip over the surface such that the bend of the cantilever, which is equivalent to the applied external force, stays constant. Although there are various ways to measure the deflection of the cantilever (*5, 27*), all commercially available instruments do this optically, either by interferometry or with displacement sensors. The resulting image is an isoforce relief of the sample. Although at the first glance one is tempted to assume that the stiffness of the cantilever would limit the applicable force, it turns out that the local forces between tip, sample, and ambient play the dominant role. In general, the long-ranged van der Waals attraction is balanced by the hard-core repulsion between tip and sample. Additional contributions stem from Coulomb interactions (*13, 28*) and from structural forces, such as hydration forces (*29*). When imaged in air, the meniscus force of a wetting water film may dominate the attraction. Because of the different characteristic decay lengths, the local forces can be only partially balanced by retracting the cantilever. Because of the long-range interactions, not only the geometry of the tip at its very end but its shape in the 10-nm scale becomes relevant (*30*). Here a counterintuitive situation emerges, that the sharper the tip is, the lower the minimum force will be. When the technique was introduced, tiny diamond chips glued onto wire springs were used. The sharpest tips are now grown onto the integrated cantilever tips by electron beam deposition (*31*) (see Fig. 1B). Besides the drastically improved aspect ratio, such tips also exhibit a much smaller curvature radius (*32*), reaching values of 10 nm and

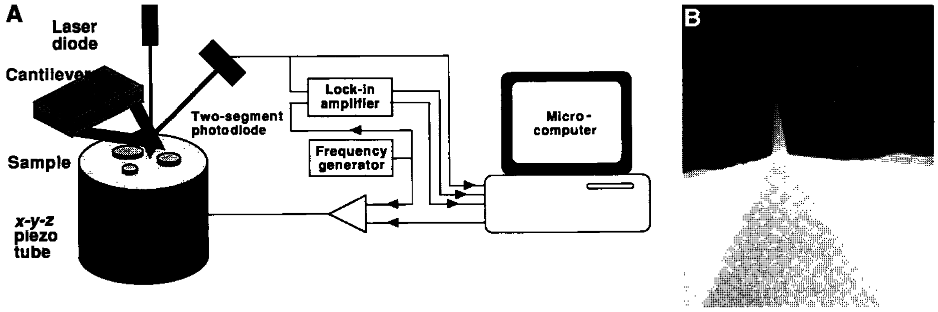

Fig. 1. (**A**) Schematics of an atomic force microscope with a beam bounce deflection sensor. Also outlined are the extensions for viscoelasticity imaging. (**B**) Carbon tip grown on top of the integrated tip of an AFM cantilever (*71*).

The authors are in the Physikdepartment, Technische Universität München, 8046 Garching, Germany.

*To whom correspondence should be addressed.